

Experimental comparison of performance degradation from terahertz and infrared wireless links in fog

Ke Su,^{1,*} Lothar Moeller,² Robert B. Barat,³ and John F. Federici¹

¹*Department of Physics, New Jersey Institute of Technology, 322 King Blvd., Newark, New Jersey 07102, USA*

²*Bell Laboratories/Alcatel-Lucent, 791 Holmdel-Keyport Rd, Holmdel, New Jersey 07733, USA*

³*Otto York Department of Chemical Engineering, New Jersey Institute of Technology, 322 King Blvd., Newark, New Jersey 07102, USA*

*Corresponding author: ks265@njit.edu

Received August 2, 2011; revised November 8, 2011; accepted November 12, 2011;
posted November 14, 2011 (Doc. ID 152166); published January 19, 2012

We describe a lab setup for analyzing impairments of terahertz (THz) and infrared (IR) free space links caused by local refraction index changes in the signal's propagation paths that could be induced by turbulence, particles, humidity, etc. A THz signal comprising a 2.5 Gb/s data load modulated on a carrier at 625 GHz, is launched through a weather emulating chamber, detected, and its performance analyzed. An IR beam at 1.5 μm wavelength carrying the same data load is superposed with the THz beam, propagating through the same weather conditions and also performance analyzed. We modulate the IR channel with a usual non-return-to-zero (NRZ) format but use duobinary coding for driving our THz source, which enables signaling at high data rate and higher output power. As both beams pass through the same channel perturbations and as their degradations are recorded simultaneously we can simultaneously compare the weather impact on both. We investigate scintillation and fog attenuation effects for the THz and IR signals by measuring bit error rates (BER), signal power, and phase front distortions. © 2012 Optical Society of America

OCIS codes: 060.2605, 040.2235, 140.3070, 060.4080, 010.1615.

1. INTRODUCTION

Edholm's law of bandwidth [1] predicts the need of data rates around 5–10 Gb/s within 10–15 years from now. The increasing demand for higher data rates suggests the development of wireless communication networks at higher carrier frequencies. Consequently, we can expect that such systems will soon push towards to the low terahertz (THz) frequency range due to its inherently larger accessible bandwidth compared to microwave and millimeter communication bands [2]. Both indoor as well as outdoor scenarios of THz communications attract much attention. Koch and his coworkers mainly focus on the experiments and simulations of THz indoor communications [3]. However, our focus is on performance degradation of outside THz communication under certain weather conditions. Towards higher carrier frequencies, THz can possibly enable reliable signaling at certain atmospheric conditions where free space infrared (IR) communication would fail. For example, attenuation by fog as well as scintillation effects due to local refraction index variations seem to have less impact on THz links than on wireless IR systems.

Research has focused on various important channels features of indoor and outdoor THz links and several experiments have been conducted, showing their potential for high data rate communications [4,5]. For example, Yamaguchi et al. [6] have developed a 120 GHz-band wireless link system which can transmit 10 Gb/s data. Ducournau et al. [7] and Nagatsuma et al. [8] have demonstrated Gb/s rates on a wireless link at 200 GHz and in the 300–400 GHz frequency band, respectively. Recently, we have developed a 2.5 Gb/s error-free transmission system [9] at a 625 GHz carrier frequency that utilizes a Schottky diodes based emitter source with re-

latively strong output power. Yamaguchi et al. [6] describe observations on how weather conditions (wind) impact the quality of the received signals and a detailed statistics for attenuation caused by rain in a 400 m link at 120 GHz carrier frequency were evaluated by Hirata et al. [10]. However, a direct experimental performance comparison between THz and IR communication links, meaning that both signals experience the same weather conditions, has not been conducted before. Most of the predictions regarding advantageous propagation features of THz beams are based on theoretical investigations originally [11,12] developed to support radio astronomy. Also, scintillation effects caused by local refractive index changes impair T-ray propagation less but limit the reach of an IR beam [13,14]. Only a few experimental reports on the degradations of THz signals in rain [10,15,16] are available. To the best of our knowledge, no experimental study of the attenuation from THz data signal in fog has been published. While it is our intention to obtain a complete description of weather impact on THz channels, we focus here on channel impairments caused by fog.

In order to study and compare propagation features of THz links with IR links under different weather conditions, we have developed a THz and IR communications lab setup with a maximum data rate of 2.5 Gb/s at 625 GHz carrier frequency and 1.5 μm wavelength, respectively. Duobinary coding of the data signal [17,18] enables emitting them from a THz source with relative high output power and narrow passband. An on/off keying modulated IR signal at 1.5 μm wavelength is superposed with this THz beam and passes through the same fog and turbulence as the THz signal. Thus performance degradations in both channels due to emulated atmospheric refraction index variations can be simultaneously recorded,

analyzed, and relative impairments quantified. We investigate attenuation and scintillation effects caused by fog through BER performance and received power levels and show for the first time how differently THz and IR communication signals are degraded when passing through the same fog conditions.

2. EXPERIMENTAL SETUP FOR THZ AND IR SIGNALING THROUGH FOG CHAMBER

The block diagram (Fig. 1) shows the main transmitter and receiver elements of our THz and IR communication links, the optics for combining both beams, our fog chamber, data acquisition interfaces, and control loops for IR power stabilization. We explain important features of the THz link followed by some remarks about the IR channel.

A. 2.5 Gb/s THz Link at 625 GHz Carrier Frequency

Our THz source (Virginia Diodes Inc.) is based on a frequency-multiplier-chain with about 1 mW output power when operated in a continuous wave (CW) mode. It consists of an amplifier driven at 2 W saturation power followed by four frequency doublers and one frequency tripler, all based on biased Schottky diodes. Its acceptance frequency band between 12.8–13.6 GHz for an applied input RF tone requires at multi Gb/s data rate to use signals with comparably narrow bandwidth such that intersymbol interference (ISI) effects caused by bandwidth reduction can remain small. Duobinary modulation yields a relatively compact spectrum compared to regular non-return-to-zero (NRZ) modulation by applying phase coding and pulse widening. Several techniques have been pro-

posed to generate duobinary modulation. We apply the delay-and-add approach. As shown in the signal modulation block of Fig. 1(a), a 2.5 Gb/s NRZ format is generated by a pulse pattern generator (PPG) with adjustable output power. The signal is divided into two replicas by means of a wideband 6 dB electrical power splitter and one branch is delayed by the duration of a bit (400 ps) with respect to the other. The replicas are combined with another 6 dB power splitter, terminated with 10 dB 50 Ohm attenuators at both inputs, in order to achieve better impedance matching and less reflections. A quasi-Gaussian low pass filter (LPF_1) with about 1700 MHz 3 dB-bandwidth is then applied to reduce the spectral width of the signal, mainly by cutting off its tail. This signal is launched into the intermediate frequency (IF) port of a double-balanced mixer where the data modulates the output of a frequency synthesizer that is connected to the local oscillator (LO) port. It is a specific feature of our double-balanced mixer that a negative input at the IF port causes a 180° phase shift of the signal at the radio frequency (RF) output and is utilized to establish the required phase coding for duobinary modulation. The data signal enters the THz source and modulates the THz radiation which emanates from the horn antenna of the THz source with 2.4 mm aperture. Note, after the first frequency doubler of the source, the duobinary phase coding is eliminated due to the squaring operation of the Schottky diode.

The output of the horn antenna is collimated by a THz lens (beam diameter ~20 mm) with short focal length (~32 mm) and transmitted over distances with up to a few meters length. After that an identical THz lens couples the beam into a receiver horn similar to the transmitter antenna whose output

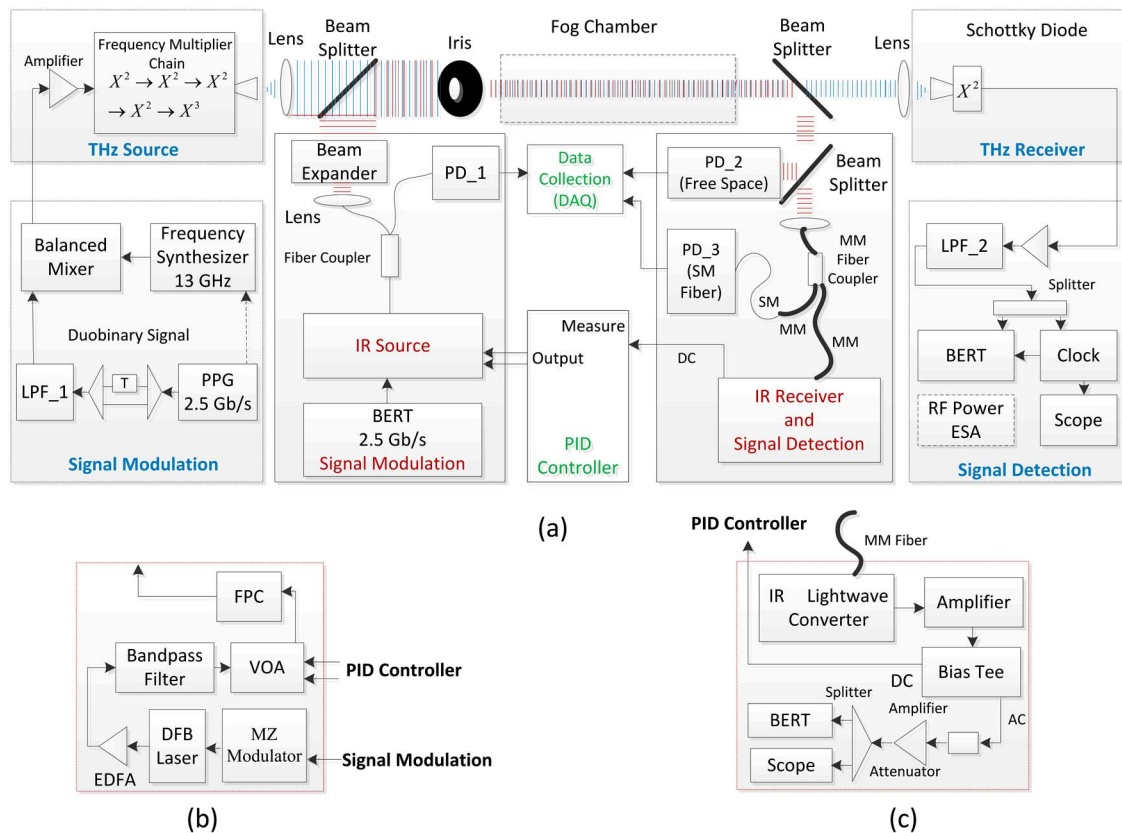


Fig. 1. (Color online) (a) Schematic diagram of THz and IR wireless communication link through fog chamber, (b) IR source, (c) IR receiver and signal detection.

is connected to a zero biased Schottky diode. The detector functions in the low power region (input power $<10 \mu\text{W}$) in good approximation as square law converter with a responsivity of about 2500 V/W at 600 GHz. The Schottky diode's output is amplified by about 42 dB using two amplifiers (80 kHz–7 GHz passband, 6 dB noise figure, maximum output power $\sim 19 \text{ dBm}$) and filtered by a quasi-Gaussian low pass filter (LPF-2) with 3 GHz 3 dB-bandwidth. A 6 dB electrical power splitter launches one output ($V_{pp} \sim 500 \text{ mV}$) to a high-speed scope or a bit error rate tester (BERT) and the other to a 2.5 Gb/s NRZ clock recovery circuit that synchronizes our measurement equipment.

Note that our current detector design, based on commercially available Schottky diodes, is suboptimal for high-speed signaling. The video resistance of the diodes, under low input power, is nominally $\sim 1.5 \text{ k}\Omega$ and connected via a series of 50 Ω transmission lines and cables to an external high-speed electrical amplifier with matched input impedance. For low speed applications and after replacing the amplifier with a high impedance device, a voltage of about 70 mV at the Schottky diode output is detectable. But with 50 Ω termination of the diode a significantly smaller voltage level is accessible at the high-speed amplifier input. A rough estimate (applying voltage divider rule 50/1550) shows thus only about 3% of the signal voltage generated in the Schottky diode is applied to the amplifier input. This mismatch degrades the noise performance of the signal launched into the BERT significantly: BER in range of 10^{-10} and higher become measurable. An iris with 8.5 mm aperture, inserted concentrically into the beam, limits its total power to an amount that results in a BER of about 10^{-7} for an unloaded fog chamber. The beam splitter and combiner, made of a thin (2 μm) nitrocellulose membrane (Thorlabs) as well as the windows of the fog chamber (15 μm polyethylene slide) reduce the signal power by no more than 2 dB.

B. 2.5 Gb/s IR Communication Link

Our IR transmitter [Fig. 1(b)] consists of a DFB Laser (wavelength $\sim 1550 \text{ nm}$), a Mach-Zehnder optical modulator, a high power erbium-doped fiber amplifier (EDFA), a narrow bandwidth optical filter ($\sim 1 \text{ nm}$ bandwidth), a low loss variable optical attenuator (VOA) and a fiber based polarization controller (FPC). All are connected by standard single-mode (SM) fiber. The beam splitting ratio is polarization dependent and we adjust the FPC for maximum detectable receiver power. The Mach-Zehnder modulator is driven by the same 2.5 Gb/s NRZ signal as our THz transmitter. An EDFA amplifies the modulator output to about 25 dBm, the maximum input power of the bandpass filter, which reduces the detection of spontaneous emission on the receiver side. After passing through the VOA, controlled by a proportional-integral-derivative controller (PID controller), the IR signal is launched into the 90:10 SM fiber coupler. Its weaker output, launched into photo detector PD_1 serves as monitor for the power entering the fog chamber. A fiber collimator expands the IR beam to about 20 mm diameter, which is comparable to the THz beam size before the iris.

The collimated IR beam is superposed with the THz beam using a beam combiner (see above) with 55% reflection ratio at 45° incident angle, transmitted through the fog chamber and deflected at its output with a similar beam splitter to spatially

separate THz and IR signals. The second beam splitter taps off a fraction of the IR power leaving the chamber and launches it towards a large area photo diode (effective area 19.6 mm^2) of detector PD_2, which in combination with PD_1 is used to determine the power loss caused by the chamber load. The remaining beam power enters via a fiber collimator a 1×2 multimode (MM) fiber coupler with 50:50 splitting ratio. Its output power is launched to a low bandwidth photo detector (PD_3) with a 1 m long standard single mode fiber (SSMF) and to a dc-coupled IR lightwave converter (Agilent 81495A) with 9 GHz bandwidth. The lightwave converter is twofold used for data detection and measuring the optical power of the incoming signal, which is accessible via general purpose interface bus (GPIB). A bias tee [Fig. 1(c)] at the converter output allows for extracting a voltage proportional to the DC components of the data signal, which serves as feedback for our PID controller of the VOA. The AC-output of the bias tee is strongly attenuated and thereafter amplified in order to level the signal-to-noise ratio (SNR) such that BERs around 10^{-7} and higher can be adjusted while satisfying the BERT requirements of input voltage swings between 250 mV and 2 V.

C. Operational Conditions of the Setup

We expect significantly higher attenuation levels for the IR signal than the THz beam when passing through fog. Simulations suggest that the losses per propagation length unit measured in dB differ by a factor between approximately 10 and 100. While in our setup power measurements can be performed easily over a dynamic range of 40 dB, BER recordings for determining the data signal quality typically cover only a few dB of receiver input power variation. In order to increase the dynamic range of the IR system for BER recordings, a proportional-integral-derivative controller (PID controller), adjusting the launched power into the chamber, is applied. Thus even at high attenuation levels the receiver power drops only insignificantly or stays constant. The controller consists of a front end with differential input amplifier (proportional control), followed by an integrator and a differentiator, arranged in what is known as 'ideal' PID topology. The output of PID controller is connected to a VOA with comparable short response time ($<10 \mu\text{s}$) but nonlinear response curve. An external voltage, equivalent to the output of IR lightwave converter for the case of an unloaded fog chamber and a BER $\sim 10^{-6}$, serves as reference for the PID controller. When fog starts to attenuate the received data signal, our control loop decreases the initially set attenuation of the VOA to keep the power level on the receiver side constant. Typically, our control loop can cover a dynamic range of about 5 to 10 dB under stable operation.

We record the output of PD_1, PD_2, and PD_3 via a DAQ board with 16 bit resolution and 1 kHz sampling rate, sufficiently high to track even the fastest fluctuations of the signals. BERs, RF power of THz signal, and optical power of the IR signal are recorded via GPIB. A LabView time controller, set to a minimum clock rate of 500 ms, which our GPIB interface can handle, synchronizes all recordings.

For an unloaded chamber we adjust the output power of the EDFA, the initial setting of the VOA, electrical attenuation at the lightwave converter output, and the aperture of the iris such that a BER of around 10^{-6} is obtained for both channels. Our BERT integrates bit errors over 500 ms. Thus at 2.5 Gb/s

data rate and the aforementioned BER, 1250 errors on average per half second are detected with a standard deviation of $\sigma = \sqrt{1250} \sim 35$ (Poisson distributed errors) i.e., with a probability of 99.7% the BER resides within an interval that corresponds to a BER fluctuation of about 16% or to an uncertainty in detected receiver power of about 0.15 dB (about 1.4%) and is comparably small in relation to other error sources contributing to the final results. In other words, statistical fluctuations of the BER at levels of 10^{-6} and higher do not significantly impact conclusions we draw from our measurement results. We chose to adjust our setup at a BER of 10^{-6} which is a typical threshold for modern forward error correction (FEC) technology used in lightwave communication systems [19].

Some atmospheric chamber designs (fog and turbulence) with control setup have been introduced by Ljaz et al. [20,21]. Our fog chamber is an opened plastic box with a dimension of $65 \times 40 \times 40$ cm³ operated at typical room atmospheric conditions and fog is generated by dripping liquid nitrogen into a cup filled with hot water (temperature about 80 °C) which is placed inside the chamber but offside with respect to the beams. The chamber has two windows on the side made of 15 μ m polyethylene foil. The fog density is controlled by the amounts of liquid nitrogen spilled into the cup. The fog density can be fluctuating over a large visibility range. We found typical visibilities varied between a few centimeters to several hundreds of meters. Measurements with a microscope suggest an average diameter of the fog drops in a range of 8 μ m. The fog diffuses into the chamber, flooding it typically in a few tens of seconds. The THz and IR beam enter the chamber via windows made of 15 μ m polyethylene foil which attenuates the beams only weakly. We did not observe condensation of fog on the windows during our experiments.

3. CHARACTERIZATION OF THE DATA LINKS BY BER MEASUREMENTS

Figure 2(a) shows for the THz channel the measured BER dependence on the detected RF power at the output of the receiver's 6 dB splitter for long ($2^{31} - 1$) and short ($2^7 - 1$) PRBS and the corresponding eye diagrams at BER = 10^{-6} . The BERT's decision threshold was optimized at a BER = 10^{-6} . Then we reduced the power of the THz signal stepwise by decreasing the aperture of the iris and measured the received power with a RF power meter.

For long PBRs and without threshold adjustment, increasing the THz power beyond a level that corresponds to a RF power of approximately -8 dBm does not reduce further the error count (error floor). But shorter patterns ($2^7 - 1$) do not show such error floor. Reasons for this can be saturation effects in the receiver Schottky diode and bandwidth limitations of the AC-coupled receiver amplifiers.

Figure 2(b) shows for the IR link the BER performance versus the received input power for same PBRs and a typical eye diagram at the input to the decision gate. As before the decision threshold was optimized at BER = 10^{-6} .

4. EXPERIMENTAL RESULTS

A. Signal Attenuation by Fog

First we show how the transmission links perform with disabled PID controller, i.e., constant IR power is launched into the chamber. As expected, when fog fume reaches the propagation path of the beams, strong attenuation of the IR light is

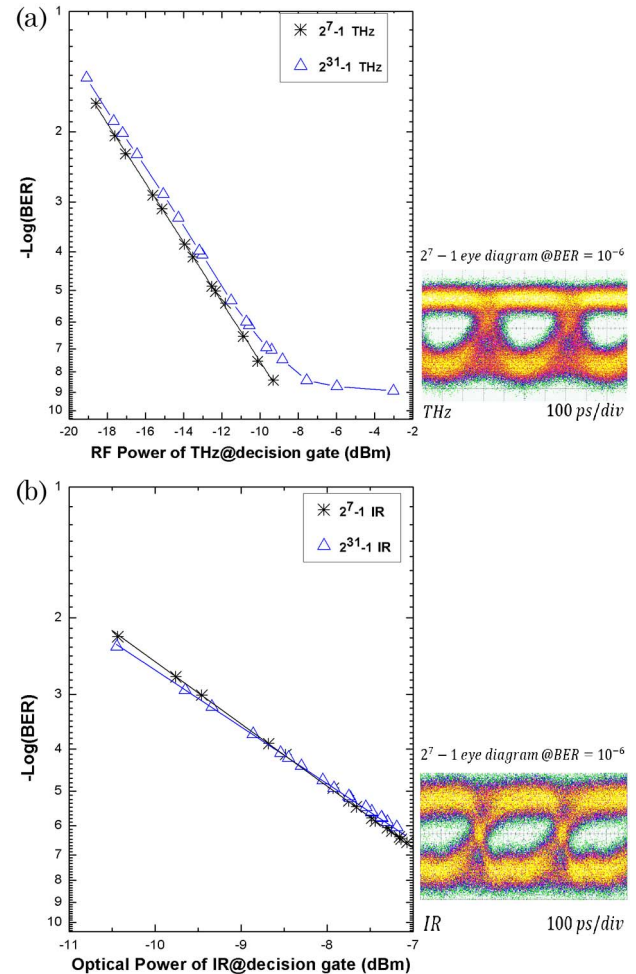


Fig. 2. (Color online) (a) BER curves of THz Link for long and short PRBSs without decision threshold optimization. Eye diagram at BER = 10^{-6} , (b) IR BER curves for long and short PRBSs with fixed decision threshold optimized at BER = 10^{-6} .

visible while the THz signal exhibits only a minor but measurable decrease in power. A typical evolution of the attenuations in both channels is shown in Fig. 3(a). Our measurement capabilities are limited to about 42 dB dynamic range during certain time intervals, as indicated in Fig. 3(a). Our recording shows the noise floor of the power meter and not the actual IR power level. Clearly there is a huge difference in the IR and THz attenuation. Usually, even 'small' amounts of fog are sufficient to block the IR beam after a few seconds of diffusion and when reaching an attenuation of about 4 dB the BER measurement of the IR signal collapses in agreement with the receiver performance shown in Fig. 3(a) and Fig. 3(b). For THz channel, a functional relation between the attenuation for both signals and the recorded BERs is clearly visible. After some tens of seconds the fog disappears into the lab environment or is converted into humidity; thus both links regain or approach their original performance, respectively. The ratio of the IR channel attenuation over the THz channel attenuation [Fig. 3(c)], both measured in dB, shows a trend to become smaller towards the end of the measurement. It will take more research to find out all underlying processes that drive this effect. But likely, fog converted into humidity during the recording time impairs the THz signal relatively stronger than

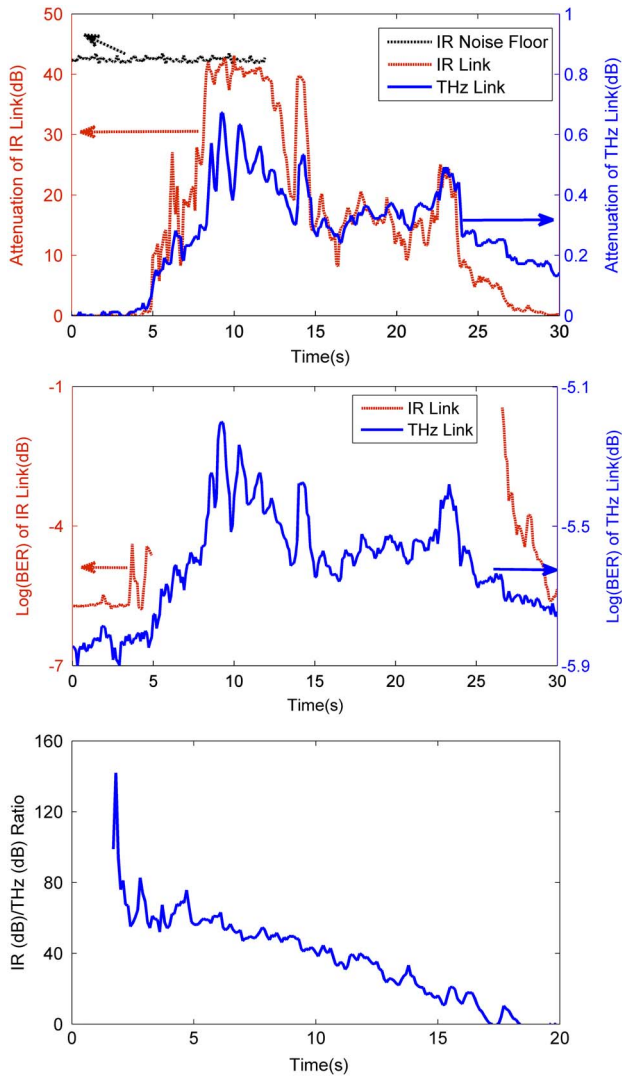


Fig. 3. (Color online) (a) Attenuation of THz link and IR link with time (b) $\log(\text{BER})$ of THz link and IR link with time (c) IR attenuation in dB relative to THz attenuation in dB over time.

the IR signal. This hypothesis is in agreement with Fig. 3(a) where the THz link towards the end of the measurement maintains a small attenuation while the IR attenuation approaches zero.

B. Scintillation Effects in Fog Chamber

Two effects caused by fog contribute to the IR power reduction on the receiver side. While attenuation of the IR beam by power decay has been demonstrated above, we discuss in the following local refraction index inhomogeneities causing phase front distortions of the optical mode that is coupled into the detector fiber. If the mode of the IR beam would be just attenuated in the fog chamber but not phase front degraded, then the IR power coupled into the receiver fiber should be in good approximation proportional to the IR power detected by PD₂. However, if phase front distortions of the IR beam occurs we expect a smaller coupling efficiency especially into SSMF with small aperture. In order to simultaneously visualize the effect of phase front distortions on the detection with large and small aperture fibers we coupled the IR signal into a 1×2 multimode power splitter whose output ports are

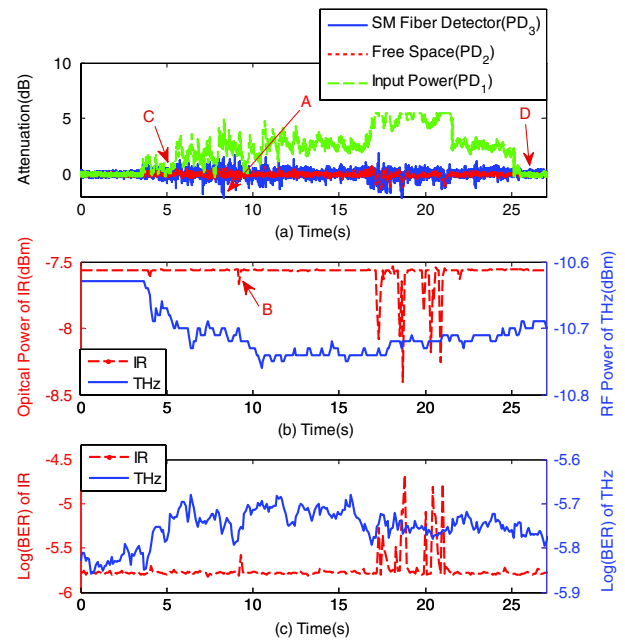


Fig. 4. (Color online) (a) Individually normalized outputs of photodetectors (PD₁, PD₂, PD₃) in dB, (b) optical power of IR and RF power of THz due to fog, (c) $\log(\text{BER})$ of IR and THz links impaired by fog.

connected to photo detector PD₃ via SSMF and our aforementioned lightwave converter with multimode fiber input.

Our goal is to keep the optical power at the data receiver's input constant by means of the PID controller when fog enters the beam so that the BER should not change (constant signal quality). The outputs of all photodetectors are simultaneously recorded along with the BER and transmitter output power of the IR channel (Fig. 4). In order to allow an easier overview on the variations of the recorded signals we plot relative changes on a decibel scale. When fog diffuses into the IR beam after about 3 s recording time, the PID controller enhances the IR power launched into the chamber and measured by photodetector PD₁. Up to about 17 s recording time our control loop can compensate the power loss inside the chamber. Thereafter, the maximum transmitter output power is insufficient to further equalize the losses of the link until the link attenuation drops back at about 22 s recording time to a level within the power margin of our system. While the detected optical power at the data receiver stays almost constant (for $t < 17$ s) we see small changes of the output of PD₂. Around pointer 'A' these variations are less than 0.15 dB but show that the receiver power and detected power of PD₂ are not always exactly proportional to each other. However, the variations of the power coupled into the SSMF appear more pronounced (up to ± 2 dB). Both, the variations in outputs of PD₂ and PD₃ indicate that scintillation effects impair the IR beam. The fog and humidity impact on the THz signal is generally small while visualization of possible scintillation effects in the THz beam is below our measurement precision. Small kinks in the received power of the data receiver (pointer 'B') could be caused by rapidly changing signal attenuation and noise which affects the stable operation of the PID controller for short time. Interestingly, at pointers 'C' and 'D' the chamber attenuation for the IR beam is almost zero whereas the attenuation of the THz signal is about 0.1 dB. Likely, at

these recording times fog was converted into humidity which impacts the IR signal comparably less than the THz signal. Our RF power meter provides a two digit reading after the comma, which explains the rough quantization of the recorded signal.

5. CONCLUSIONS

We have reported a lab setup that allows us to experimentally investigate impairments on THz and IR free space links caused by local refraction index changes in the propagation medium. Two 2.5 Gb/s data signals modulated on a THz and IR carrier are propagating through the same space volume and are by BER and power measurements performance characterized after detection. We found that the attenuation levels for the IR beam are typically several orders of magnitude higher than those for the THz beam when both signals propagate over distances of about a 1 m and through the same fog. We were able to demonstrate that the IR signal is impaired by both attenuation and scintillation effects whereas the THz signals experiences just attenuation. While in our setup the IR scintillation effects are small they can accumulate in real links over longer transmission distances and limit the system's BER performance. Here we demonstrate that an advantage for THz links compared to IR links is that they are less susceptible to fog attenuation and scintillation. The magnitude of scintillation effects depends on the fog distribution within the propagation path, which is difficult to control. However, as both signals pass the same fog fluctuations simultaneously, their relative impairment on both beams becomes accessible and comparable.

ACKNOWLEDGMENTS

This material is based upon work supported by the National Science Foundation under Grant No. ECCS-1102222.

REFERENCES

1. S. Cherry, "Edholm's law of bandwidth," *IEEE Spectrum* **41**, 58–60 (2004).
2. P. Zhouyue and F. Khan, "An introduction to millimeter-wave mobile broadband systems," *IEEE Commun. Mag.* **49**, 101–107 (2011).
3. C. Jansen, R. Piesiewicz, D. Mittleman, T. Kurner, and M. Koch, "The impact of reflections from stratified building materials on the wave propagation in future indoor terahertz communication systems," *IEEE Trans. Antennas Propag.* **56**, 1413–1419 (2008).
4. J. Federici and L. Moeller, "Review of terahertz and subterahertz wireless communications," *J. Appl. Phys.* **107**, 111101 (2010).
5. T. Kleine-Ostmann and T. Nagatsuma, "A review on terahertz communications research," *J. Infrared Millim. Terahertz* **32**, 143–171 (2011).
6. R. Yamaguchi, A. Hirata, T. Kosugi, H. Takahashi, N. Kukutsu, T. Nagatsuma, Y. Kado, H. Ikegawa, H. Nishikawa, and T. Nakayama, "10-Gbit/s MMIC wireless link exceeding 800 meters," in *Radio and Wireless Symposium* (IEEE, 2008), pp. 695–698.
7. G. Ducournau, P. Szriftgiser, D. Bacquet, A. Beck, T. Akalin, E. Peytavit, M. Zaknourne, and J. F. Lampin, "Optically power supplied Gbit/s wireless hotspot using 1.55 μm THz photomixer and heterodyne detection at 200 GHz," *Electron. Lett.* **46**, 1349–1351 (2010).
8. T. Nagatsuma, H. J. Song, Y. Fujimoto, K. Miyake, A. Hirata, K. Ajito, A. Wakatsuki, T. Furuta, N. Kukutsu, and Y. Kado, "Giga-bit wireless link using 300–400 GHz bands," in *MWP'09. International Topical Meeting on Microwave Photonics* (Academic, 2009), pp. 1–4.
9. L. Moeller, J. Federici, and K. Su, "2.5 Gbit/s duobinary signaling with narrow bandwidth 0.625 terahertz source," *Electron. Lett.* **47**, 856–858 (2011).
10. A. Hirata, R. Yamaguchi, H. Takahashi, T. Kosugi, K. Murata, N. Kukutsu, and Y. Kado, "Effect of rain attenuation for a 10-Gb/s 120-GHz-band millimeter-wave wireless link," *IEEE Trans. Microwave Theory Tech.* **57**, 3099–3105 (2009).
11. C. M. Mann, "Towards terahertz communication systems," in *Terahertz Sources and Systems*, R. Miles, P. Harrison, and D. Lippens, eds. (Academic, 2001), pp. 261–267.
12. M. J. Rosker and H. B. Wallace, "Imaging through the atmosphere at terahertz frequencies," in *IEEE/MTT-S International Microwave Symposium* (IEEE, 2007), pp. 773–776.
13. L. C. Andrews and R. L. Phillips, *Laser Beam Propagation Through Random Media* (Academic, 1998).
14. L. C. Andrews, R. L. Phillips, and C. Y. Hopen, *Laser Beam Scintillation with Applications* (Academic, 2001).
15. T. Utsunomiya and M. Sekine, "Rain Attenuation at 103 GHz in Millimeter Wave Ranges," *Int. J. Infrared Milli.* **26**, 1651–1660 (2005).
16. S. A. Khan, A. N. Tawfik, C. J. Gibbins, and B. C. Gremont, "Extra-high frequency line-of-sight propagation for future urban communications," *IEEE Trans. Antennas Propag.* **51**, 3109–3121 (2003).
17. A. Lender, "The duobinary technique for high-speed data transmission," *IEEE Trans. Commun. Electron.* **82**, 214–218 (1963).
18. D. Penninckx, M. Chbat, L. Pierre, and J. P. Thiery, "The phase-shaped binary transmission (PSBT): a new technique to transmit for beyond the chromatic dispersion limit," in the 22nd European Conference on Optical Communications (ECOC 22) (Academic, 1996), pp. 173–176.
19. T. Mizuochi, "Recent progress in forward error correction and its interplay with transmission impairments," *IEEE J. Quantum Electron.* **12**, 544–554 (2006).
20. H. Le-Minh, Z. Ghassemlooy, M. Ijaz, S. Rajbhandari, O. Adebajo, S. Ansari, and E. Leitgeb, "Experimental study of bit error rate of free space optics communications in laboratory controlled turbulence," in *GLOBECOM Workshops* (IEEE, 2010), pp. 1072–1076.
21. M. Ijaz, Z. Ghassemlooy, H. Le Minh, S. Rajbhandari, J. Perez, and A. Gholami, "Bit error rate measurement of free space optical communication links under laboratory-controlled fog conditions," in 16th European Conference on Networks and Optical Communications (NOC) (Academic, 2011), pp. 52–55.